TECHNICAL INFORMATION SERIES

TRANSITION OF THE HYPERSONIC BOUNDARY LAYER ON A CONE

Part II: Experiments at M = 10 and More on Blunt Cone Transition

SPACE SCIENCES LABORATORY

SPACE SCIENCES LABORATORY

EXPERIMENTAL FLUID PHYSICS SECTION

TRANSITION OF THE HYPERSONIC BOUNDARY LAYER ON A CONE:

PART II - EXPERIMENTS AT M = 10 AND MORE ON BLUNT CONE TRANSITION

by

Eric J. Softley*

This work was performed for SAMSO, USAF under Contract AF 04(694)-772 and was declassified in accordance with instructions received July 29, 1968 from the office of Information, Space and Missile Systems Organization, USAF.

R68SD14

October, 1968

*now in Re-Entry Systems, MSD

MISSILE AND SPACE DIVISION

GENERAL ELECTRIC

BLANK PAGE

CONTENTS

Summary

Observation of transition of the hypersonic boundary layer on a cone continued with experiments at $M_\infty = 10$. Transition independent of the unit Reynolds number was obtained. This is dramatically different from the results obtained earlier. Blunt cone transition with a wide range of nose radii was examined. It was found possible to correlate transition on different blunt cones using a new bluntness parameter S_B/S_{cr}.

List of Figures

Notation

C_H	Non-dimensional heat transfer rate (Stanton number)
M	Mach number
P (LB/IN^2)	Pressure
$\dot{q}$ (BTU/FT^{2}SEC)	Heat transfer rate (or $\dot{Q}$)
R (IN)	Radius
Re	Reynolds number
S (FT)	Distance along cone surface from stagnation point (wetted length)
T (^{o}K)	Temperature
U (FT/SEC)	Velocity
X (FT)	Distance along cone axis from virtual apex

Subscripts

B	at beginning of transition
c	cone
cr	at location where $M_e = \hat{M}_e - 1$
E	at end of transition
e	at edge of boundary layer
N	nose of model
R	recovery value
w	wall or surface value

sw	at location where boundary layer swallows nose induced entropy layer ($M_e = 0.95\ \hat{M}_e$)
0	total value
5	reflected region of shock tunnel
∞	ahead or outside of cone shock

Superscript

'	behind normal shock
^	on sharp cone

Abbreviation*

VIZAAD	Viscous Interaction Zero Angle of Attack Drag
NSBL	Non-Similar Boundary Layer

*These are two blunt cone flow field computer programs.

BLANK PAGE

1. INTRODUCTION

Experiments on hypersonic boundary layer transition in the GE 6"/54" shock tunnel at free stream Mach numbers of 12 and 15 have already been reported (1). The range of parameters covered were limited by the tunnel capability (see Fig. 1). The largest operating capability occurs at the lower Mach number and lowest stagnation temperature for a sharp cone. Increasing the total temperature (lower wall temperature ratio) or the nose radius increases the free stream transition Reynolds numbers. At a free stream Mach number of 15 very little parameter variation is possible.

A logical extension to these results would then be at a lower free stream Mach number. The physically largest possible throat size allows a free stream Mach number of around 10. Some experiments were performed with this throat using the same basic 12 ft. cone model used earlier. Some re-design of the model was necessary since transition could now take place at the extreme forward section of the model which had not been instrumented in sufficient detail.

2. EXPERIMENTAL DETAILS

The flow fields are determined as before by surface pressure measurements on the model and the data is shown in Figure 2 together with the corresponding local Mach number calculated from the surface pressure data. This has been described in earlier reports of the higher Mach number data. It should be pointed out that since this condition represents a further decrement away from the design condition of the

tunnel, (M = 20), a slightly increased edge Mach number gradient exists for this case. Since the scale of the experiment is generally smaller because of the increase in the unit Reynolds number, the actual change in edge properties represents about the same percentage changes in Mach number for the higher Mach number data.

The model was modified by replacing the uninstrumented nose section with sections containing detailed instrumentation. Figure 3 demonstrates the modified nose sections. Because of the small diameter at this location, it was not possible to use gages of the type previously used in the model. Hence it was decided to use continuous pyrex strips in the model with the pyrex forming part of the model surface. The strips were then drilled ultrasonically for the gage wires and painted with the gage materials. It was thus possible to obtain the fine spacing on the heat gages shown in Figure 3. The cross-section of the construction is shown in Figure 4. The pyrex T-section was ground with a steel dummy model so that the surface match from gage to model was such that no measurable step was obtained. It was also necessary to add additional internal amplifiers and these were located just behind the first two instrumented sections of the model. Existing instrumentation to 12 feet on the cone was also available. For the large bluntness experiments the new nose sections were not, of course, used. Indeed transition was generally then on the back portion of the cone.

Because of funding limitations on the experiment, the parameters

varied were the wall temperature ratio and the nose bluntness only. It was unfortunately not possible to obtain profiles and spectral measurements. The instrumentation therefore was restricted to surface pressure and surface heat transfer gages. Transition was again determined from the surface heat transfer measurements.

In common with most of the thinking on transition, local properties are quoted in correlation of blunted cone data. In Ref. 1 the GE blunt cone calculation known as VIZAAD (2) was used to calculate local properties. This approach uses boundary layer correlations to estimate the all important boundary layer thickness. Profiles of pitot pressure and total temperature obtained through the boundary layer on this 12 ft. cone has been compared (3) with another calculation denoted NSBL (for non-similar boundary layer) (see Ref. 4). For continuity VIZAAD was used again to calculate local properties. A comparison between these various approaches is given later.

3. SHARP CONE TRANSITION

The test results of $M_\infty = 10$ are summarized in Tables I-III. The free stream conditions are shown in Table I. The table itemizes conditions at the apex of the sharp cone. Due to the Mach number gradient all of the properties change as X increases.

The surface heat transfer data is used to determine X_B and X_E, the axial locations of the beginning and end of transition. At a fixed wall temperature ratio a unit Reynolds number variation is obtained by changing pressure levels. Some results are shown in Figure 5 where C_H, the

non-dimensional heat transfer is considered a function of Re_x. A clear Re_{x_B} is determined for two of the cases. For the third case the flow was laminar up to the same Re_{x_B} (end of measuring region). The data at condition 16, however, (Fig. 6) shows a curious anomaly which was not present at higher Mach numbers or at any of the other flow fields. The heat gages demonstrated a break away of heat transfer from laminar level at a different location from that obtained by extrapolating back the heat transfer data immediately before the end of transition. No physical explanation for this is yet known.

From these four flows, all obtained at a wall temperature ratio of 0.26, it was possible to obtain transition Reynolds number as a function of the unit Reynolds number in the free stream (see Fig. 7). The lines marked 12.2 and 10.2 are for data obtained in this facility at the higher free stream Mach numbers on the same cone. Also shown is the trend of anticipated results at free stream Mach number of 10 corresponding to an edge Mach number of about 8.8. Notice that the actual data obtained give the same Re_{x_B} for a wide range of unit Reynolds numbers and therefore certainly do not fit the anticipated results. The data then represent a dramatic change from that observed earlier in most wind tunnels, and even in a ballistic range (Ref.11) in that transition independent of the unit Reynolds number was obtained. Notice that condition 16 represents two transition data points since two separate definitions of transition are possible. The two points, X_{B_1} and X_{B_2} are shown in Figure 7. It

may or may not be coincidental that X_{B_1} fits the "anticipated" trend.

At other wall temperatures, two data points were obtained. Since so little data is present, it will certainly be rash to claim a wall temperature effect with the data shown in Figure 8. It is true, however, that different wall temperature data do not fit the same unit Reynolds number trend as they did at $M_\infty = 12$ and 15. It is possible to combine one of the condition 16 points with the other wall temperature points to produce a unit Reynolds number effect independent of wall temperature. However, this is only one of several possible results. We conclude at the present time that more data and information are needed to determine whether there is a wall temperature effect associated with the Mach 10 data in this tunnel.

Recently Mateer and Larson (5) reported some new results on cone transition in a NASA-Ames blowdown tunnel. The 5° cone data falls within our definition of slender cone ($\vartheta_c < 10^\circ$). For this configuration there was little or no influence of unit Reynolds number on transition. This data is represented on our transition correlation shown in Figure 9.

Without more experiments it is possible to only suggest a reason for the lack of unit Reynolds number effect for these two examples. Mateer and Larson suggested that a helium layer on the nozzle walls (used for nozzle cooling) reduces the noise radiated from the tunnel nozzle boundary layer. Pate and Schueler (10) have recently given strong evidence of the influence of such radiated noise.

For the shock tunnel experiments at $M_\infty = 10$ the only physical change

was in nozzle throat diameter. Since there will still be nozzle radiated noise, although non-dimensionally less than at higher Mach numbers, the lack of unit Reynolds number influence is not obvious. One can postulate that some other source of free stream turbulence, possibly generated in the reflected region of the tunnel, becomes the controlling factor at $M_\infty = 10$. Some experiments are presently being conducted to examine this possibility.

The drastic difference in unit Reynolds number effect from $M_\infty = 12$ and 15 to $M_\infty = 10$ in one tunnel underscores the comments made in Ref. 1 concerning the effect of Mach number on sharp cone transition. Using the same "chosen" unit Reynolds number of 2×10^6 the correlation of transition Reynolds number with Mach number appears in Figure 10. With the addition of the 5° cone results of Mateer and Larson (5) plus the information from Stainback (6) that his tunnel appears "excessively noisy" the Mach number curve is now somewhat different from that shown in Ref. 1. The new relationship has a strong Mach number effect only at high edge Mach numbers.

However, it is clear from Figure 8 that the choice of unit Reynolds number is very much a feature of this "Mach number effect." Hence, as indicated in Ref. 1, this "effect of Mach number" should be noted with extreme caution and is really at best qualitative at this stage.

4. BLUNT CONE TRANSITION

4.1 Results at $M_\infty = 10$ and 12

The blunt cone experiments were in two series. A small nose bluntness

variation was obtained using the modified nose model described earlier. These results are in Table III. Maximum nose radius was .050". In addition, some experiments with the original configuration and large nose radii (.5" to 1.0") were performed and also tabulated in Table III. As explained earlier the VIZAAD flow fields were used for data evaluation. Some discussion will be made later on the importance of the calculation technique on the conclusions.

With a given free stream and cone angle the transition location depends on the nose radius. Using the free stream nose Reynolds number as a parameter the location of transition is demonstrated in Figure 11. Data obtained at both Mach 10 and Mach 12 appear to give the same relationship for $S_B/\hat{S}_B$. As the nose radius increases the location of transition moves back about a factor of 6 in transition length, the trend then reverses steeply. The reversal takes place at the location where the swallowing distance crosses the transition location, i.e. for S_B/S_{sw} of unity. The change in characteristics as the transition location goes past the swallowing distance is sufficiently great that it is convenient to label the two regions differently, namely "small bluntness" for the case where transition is behind the swallowing distance and "large bluntness" where transition is in front of the swallowing distance. Figure 12 shows these same two regions in terms of the local transition Reynolds number. Note that the increase in transition Reynolds number from sharp cone to the maximum value is about a factor of 2 in Reynolds number. The "large bluntness" characteristic has been extended

to a decrease of over an order of magnitude in Reynolds number.

It has been suggested by Stetson and Rushton that a parameter for measuring bluntness is the ratio of the transition location to the swallowing distance, S_{sw}. The data shown for both Mach 10 and 12 is demonstrated in Figure 13 with the ratio of transition Reynolds number on the blunt cone to that on the sharp cone is considered a function of the transition location over the swallowing distance. The data does correlate for differing Mach numbers and nose radii. However, this does not really represent any particular improvement in correlation unless it proves to be unique for different cone angles and different Mach numbers. There will later on be a comparison between this data and that of Stetson and Rushton (9) at Mach 5.5 for an 8^{o} cone.

4.2 Methods of Calculation of Blunt Body Boundary Layers

Correlation of blunt body transition data is often made in terms of local Reynolds number, Mach number etc. Even for a simple configuration like a sphere cone the flow field calculation is quite complex since there are two major problems,namely the calculation of an entropy layer due to the blunt nose and the calculation (under varying edge conditions) of a boundary layer within this entropy layer. Figure 22 shows a sketch of the flow field which is typical of this configuration. For the inviscid blunt body flow field the calculation of the different regions has been the object of much theoretical work. The region in the vicinity of the nose represents a difficult mathematical problem. The flow is subsonic and

the partial differential equation for the steady flow problem is elliptic. The correct boundary conditions should be defined on a known closed boundary. In practice, part of the boundary is not known, i.e. the shock wave and the method of calculation of the shock layer knowing only one boundary and the conditions along it(namely the body)has been the source of many approximate methods. It has been shown that an exact solution is obtained by considering the unsteady problem in which the shock wave formation is part of the problem. If this is done the flow equation is hyperbolic and the problem is well defined.

Amongst the direct approaches to the steady problem is a method of relaxation developed by Gravalos (7). From this it is possible to calculate the solution in the vicinity of the nose and using the method of characteristics the solution in the supersonic region following the nose. The work has been developed to the point where the flow field solution has been programed on large digital computers.

Using this derived blunt body flow field the second problem that arrives is that of calculating the boundary layer. Studerus and Dienna (2) developed a program for the calculation of the boundary layer on a sphere cone body using correlations for the boundary layer thickness developed by Walker (8). A mass balance is used to find the stream line from the edge of the boundary layer and its location as it crosses the shock wave. This method denoted VIZAAD has been used in earlier calculations of the blunt body transition data. The input to the calculations were the free

stream conditions and the pressure distribution on the cone. It is noted that since the nozzle of the tunnel was not operated at the design flow condition a residual gradient occurs and hence the pressure on the body is an important input to the problem.

It is apparent that the accuracy of the above method is very dependent on the estimation of boundary layer thickness. More recently a calculation developed by Levine (3) and denoted NSBL (non-similar boundary layer) calculates the boundary layer by integrating step by step from the nose within a previously calculated blunt body flow field. The full boundary layer equations are calculated and complete profiles of information are available step by step along the cone. A comparison between the two above techniques for two examples of flow in the GE tunnel is shown in Figures 14 and 15. The free stream Mach number is approximately 10 (with a gradient as observed earlier) and the sharp cone Mach number would be approximately 9 at the end of the cone. Two examples, namely that of 1/2 inch and 1 inch nose radius, are shown and are typical of the large bluntness. The maximum discrepancy for the two calculations was about 5% in edge Mach numbers. For the Reynolds number the non-similar boundary layer predicted edge Reynolds number somewhat above those of the VIZAAD calculation with the maximum difference being 15%.

For many of the transition experiments the beginning of transition was behind the swallowing distance. The discrepancy between the calculations is very much smaller for this region being typically 2% in M_e

and 5% in Re_s. It is concluded that the choice of calculations when applied to the data in Figures 11 and 13 does not influence the trends in the data or the conclusions reached.

In Ref. 4 the author compared the NSBL calculation with experimental profiles. There was generally excellent agreement between the two. As an indication of the relative values obtained in this comparison

$X = 5.0$ ft. $\quad R_N = 0.5''$

$\delta \sim 1/2\ \delta_e$ (entropy layer thickness)

$M_e = 6.7$ from VIZAAD calculation

$M_e = 6.4$ from NSBL calculation

$M_e = 6.8 \pm 0.3$ from experimental profiles

From the little experimental information available it was concluded that the VIZAAD calculation gave edge Mach numbers that agreed with the experiment within the experimental scatter.

4.3 Recalculation of Blunt Cone Transition Data of Stetson and Rushton (Ref. 9)

The transition data reported by Stetson and Rushton (9) includes an important study of the influence of bluntness on transition. The free stream Mach number was 5.5 and cone half angle was 8°. The author assumed, as a basis of their calculations, a linear Mach number variation along the cone. In Figure 16 is shown a comparison for a calculation of the swallowing distance. The VIZAAD computed values correlate on a single curve, $S_{sw} = S_{sw}(R_N \cdot Re_{\infty N})$. The values used by Stetson and Rushton are

somewhat more scattered but generally 30% larger.

The edge Mach number shows significant differences (Fig. 17). The Reynolds numbers also will then be different. It was felt that for consistency a recalculation of the data of Ref. 9 was needed before a comparison was made with the data at higher free stream Mach numbers. A complete flow field calculation was made for each blunt body experiment. The results are listed in Table V.

In Figure 18 the transition location is shown to increase with increasing bluntness with the maximum delay a factor of 4 over the sharp cone value. However, using the new flow field calculation it is found that the transition Reynolds number also increases as the nose radius is increased as shown in Figure 19 with the maximum increase in transition Reynolds number approximately a factor of 2 over the sharp value. The bluntness parameter used here is the ratio of transition location over the swallowing distance. Similar to the results at higher Mach number it is possible to divide the blunt transition results into two distinct regions corresponding to "small bluntness" and "large bluntness" with the same trends as at higher M_∞ (see Figs. 11 and 12). It is found that the cross-over point for the two sets of data occurs when $S_B/S_{sw} \sim 1/2$. This is also demonstrated in Figure 18 where it is seen that the computed swallowing location crosses the transition location before the transition location reaches a maximum.

If the data of Stetson and Rushton is compared with that obtained

in the GE shock tunnel it is found that the two regions, "small bluntness" and "large bluntness", with the same characteristics, are both represented. This is even more obvious if the edge Mach number is used as dependent parameter. Figure 20 shows the three experimental blunt cone cases compared to the sharp cone transition. A maximum transition Reynolds number due to bluntness, which is about a factor of 2 above the sharp cone value, is suggested. It is apparent that M_e and Re_s alone are insufficient to obtain a correlation of blunt cone transition at high free stream Mach numbers. A better approach would appear to be M_e (sharp) and some bluntness parameter.

From Figure 13 and 14 it is clear that the parameter S/S_{sw} does not uniquely describe the movement of transition with bluntness. In Figure 26 of Ref. 1 it was demonstrated that sharp cone transition occurs in the outer edge of the boundary layer, presumably at the radial location where the disturbance is sonic with respect to the inviscid flow. On the forward portion of the blunt cone the boundary layer edge Mach number and velocity are reduced by the entropy change produced by the blunt shock. It is possible to introduce a location S_{cr} where the local edge is sonic with respect to the outer edge of the entropy layer. It is convenient for correlation purposes to define S_{cr} as the location where $M_e = \hat{M}_e - 1$ (note that for S_{sw}, $M_e = .95\,\hat{M}_e$). As long as $S_B > S_{cr}$ there exists some point in the boundary layer where the flow is sonic with respect to the flow outside the entropy layer. This suggests that S/S_{cr} may determine the

turning point for the two bluntness regions.

Figure 21 shows the result of using S_B/S_{cr} as the bluntness parameter. For small bluntness the transition data for the three studies fit a single correlation within about $\pm$ 20%. For a small region of the large bluntness S_B/S_{cr} 0.2 this is still true. For large bluntness some other factor presumably is better suited. Of more importance is the fact that the maximum Reynolds number point occurs at the same S_B/S_{cr} ($S_B/S_{cr} \sim 1$).

5. CONCLUSIONS

1. It has been demonstrated that it is possible to obtain transition results on a sharp slender cone in one facility which demonstrate both a unit Reynolds number sensitivity and a lack of same. In this instance the only change in tunnel operation was an increase in throat size, and hence a decrease in Mach number over the cone.

2. A reconsideration of the available sharp cone transition data suggests that the strong Mach number influence on transition exists for $M_e > 8$. The unit Reynolds number influence is much smaller than the Mach number influence in this region.

3. The little data available on the blunt cone transition at high free stream Mach numbers is quite consistent. For a region of "small bluntness", $S_B > S_{cr}$, transition moves back and the transition Reynolds number increases with increasing bluntness. For a region of "large bluntness", $S_B < S_{cr}$, this process is sharply reversed. A maximum transition Reynolds number due to bluntness which is about a factor of two over

sharp slender cone transition is postulated. The use of edge Mach number to correlate transition seems ill-advised. The sharp cone edge Mach number and the bluntness parameter S_B/S_{cr} better describe the phenomena.

References

1. Softley, E.J., Graber, B.C. and Zempel, R.E., "Transition of the Hypersonic Boundary Layer on a Cone, Part I Experiments at M_∞ = 12 and 15", GE TIS R67SD39.

2. Studerus, C.J. and Dienna, E.A., "Viscous Interaction Zero Angle of Attack (VIZAAD) Program", GE TIS R64SD292, Nov. 1964.

3. Levine, J.N., "Finite Difference Solution of the Laminar Boundary Layer Equations Including the Effects of Transverse Curvature, Vorticity, and Displacement Thickness", GE TIS R66SD349, Dec. 15, 1966.

4. Softley, E.J. and Sullivan, R.J., "Theory and Experiment for Some Non-Similar Hypersonic Boundary Layers", AGARD Specialists Meeting on "Hypersonic Boundary Layers and Flow Fields", London, May 1968.

5. Mateer, G.M. and Larson, H.K., "Unusual Boundary Layer Transition Results on Cones in Hypersonic Flows", AIAA Paper 68-40, Jan. 1968.

6. Stainback, P.C., (private communication).

7. Gravalos, F.G., Edelfelt, I.H. and Emmons, H.W., "The Supersonic Flow Field About a Blunt Body of Revolution for Gas at Chemical Equilibrium", Proc. 9th Annual Congress IAF, Aug. 1958.

8. Walker, G.K., "The Growth of Laminar Boundary Layers with Zero Pressure Gradient", GE RST Thermodynamics Fundamental Memo, TFM-8151-008, Jan. 1963.

9. Stetson, K.F. and Rushton, G.H., "A Shock Tunnel Investigation of the Effects of Nose Bluntness, Angle of Attack and Boundary Layer Cooling on Boundary Layer Transition at a Mach Number of 5.5", AIAA Paper No. 66-495.

10. Pate, S.R. and Schueler, C.J., "An Investigation of Radiated Aerodynamic Noise Effects on Boundary-Layer Transition in Supersonic and Hypersonic Wind Tunnels", AIAA Paper No. 68-375.

11. Potter, J.L., "Observation on the Influence of Ambient Pressure on Boundary Layer Transition", AIAA Journal, Vol. 6, pp. 1907-1911, Oct. 1968.

The following have been quoted for transition data:

12. Maddalon, D.V. and Henderson, A., Jr., "Boundary Layer Transition at Hypersonic Mach Numbers", AIAA Paper 67-130, Jan. 1967.

13. McCauley, W.D., Saydah, A. and Bueche, J., "The Effect of Controlled Three Dimensional Roughness on Hypersonic Laminar Boundary Layer Transition", AIAA Paper No. 66-26.

14. Sanator, R.J., DeCarlo, J.P. and Torrillo, D.T., "Hypersonic Boundary Layer Transition Data for a Cold-Wall Slender Cone", AIAA Journal, pp. 758-760, April 1965.

TABLE I

FREE STREAM CONDITIONS AT X = 0 ($M_\infty \approx 10$)

COND	P_5	T_5	M_∞	ρ_∞	U_∞	P_∞	T_∞	$\frac{\rho_\infty U_\infty}{\mu_\infty}$
	lb/in^2	^oK		lb/ft^3 $x10^4$	ft/sec	lb/in^2 $x10^2$	^oK	Re/ft $x10^{-5}$
15	4500.	1298.	9.82	24.4	5516	11.95	72.7	40.5
16	1500.	1336.	9.50	9.01	5484	4.62	76.7	14.0
17	500.	1342.	9.12	3.56	5447	1.95	82.1	5.2
18	1000.	1063.	9.64	8.28	4685	3.01	54.3	16.4
19	3000.	2950.	9.12	5.53	8632	7.67	206.5	4.6
20	1000.	1297.	9.30	7.00	5371	3.61	76.9	10.6

TABLE II

SHARP RESULTS AT $M_\infty = 10$

COND	X_B	$M_{\infty B}$	M_{e_B}	Re/ft	Re_{S_B}	Tw/T_R	$Re_{\infty N}$
	(ft.)			$\times 10^{-6}$	$\times 10^{-6}$		
15	.84	10.0	8.8	5.2	4.4	.26	400
16	2.35 (1.75)*	9.9 (9.9)	8.8 (8.8)	1.7 (1.8)	4.0 (3.1)	.26 (.26)	140 (140)
17	8.0	10.4	9.0	.52	4.2	.26	50
18	1.6	9.9	8.7	2.1	3.3	.33	160
19	4.5	9.9	8.7	.59	2.7	.12	50
20	3.8	10.0	8.7	1.2	4.5	.26	100

*See Text

TABLE III

BLUNT RESULTS AT $M_\infty = 10$

$Tw/T_R = 0.26$

R_N	Nominal M	X_B	S_B	X_{sw}	X_B/X_{sw}	M_{e_B}	Re_{S_B}	Re_{∞_N}
(in)		(ft)	(ft)	(ft)			$\times 10^{-6}$	
.01	10	2.5	2.51	0.05	50.0	8.61	4.0	1.16×10^3
.02	10	3.0	3.01	0.15	20.0	8.55	4.8	2.32×10^3
.05	10	3.6	3.61	0.84	4.3	8.51	5.8	5.8×10^3
0.5	10	>12.0	>12.0	18.0	0.67	6.4	5.7	1.2×10^5
0.5	10	8.5	8.2	18.0	0.47	5.9	3.6	1.3×10^5
0.75	10	9.5	9.0	26.0	0.36	5.4	2.75	1.8×10^5
0.75	10	6.0	5.5	30.0	0.20	4.5	1.45	2.4×10^5
1.0	10	4.7	4.1	40.0	0.12	4.0	0.56	2.6×10^5

TABLE IV

BLUNT RESULTS AT $M_\infty = 12$

(Data from Ref. 1)

R_N	Nom. M_∞	$\frac{Tw}{T_R}$	X_B	S_B	X_{sw}	X_B/X_{sw}	M_{e_B}	Re_{S_B}	Re_{∞_N}
(in)			(ft)	(ft)	(ft)			$\times 10^{-6}$	
0.1	12	.26	4.0	3.9	2.25	1.78	9.9	7.7	1.65×10^4
0.1	12	.26	5.6	5.5	1.70	3.3	10.1	6.8	1.0×10^4
0.1	12	.26	7.5	7.4	1.25	6.0	10.2	5.6	6.2×10^3
0.1	12	.21	4.4	4.3	1.85	2.4	9.9	6.0	1.3×10^4
0.1	12	.21	7.2	7.1	1.40	5.1	10.1	5.8	7.7×10^3
0.172	12	.26	4.9	4.8	4.1	1.2	9.8	8.7	2.9×10^4
0.172	12	.26	6.5	6.4	3.0	2.2	10.1	7.3	1.7×10^4
0.172	12	.26	8.0	7.9	2.4	3.3	10.2	5.6	1.05×10^4
0.172	12	.21	5.7	5.6	3.5	1.6	9.9	7.1	2.2×10^4
0.172	12	.21	9.7	9.6	2.65	3.6	10.2	7.2	1.3×10^4
0.3	12	.26	8.3	8.1	7.5	1.1	9.6	10.1	5.0×10^4
0.3	12	.26	9.5	9.2	5.7	1.7	10.2	8.7	3.0×10^4
0.5	12	.26	>12	>12	12	>1.0	> 8.6	>10.0	8.2×10^4

TABLE V

STETSON & RUSHTON BLUNT CONE DATA RECOMPUTED BY VIZAAD

$M_\infty = 5.5 \quad \vartheta_c = 8^\circ$

R_N	S_B	S_{sw}	M_e	Re_{S_B}	$Re_{\infty N}$
(ft)	(ft)	(ft)		$x10^{-6}$	$x10^{-4}$
.00260	.87	.30	4.83	3.13	0.70
.00260	.83	.31	4.83	3.00	0.70
.00520	.89	.73	4.76	2.85	1.30
.00520	1.04	.76	4.80	3.69	1.40
.00520	1.00	.73	4.80	3.05	1.20
.00781	1.17	1.30	4.65	3.64	2.03
.00781	1.67	1.19	4.81	3.37	1.25
.00781	1.21	1.35	4.66	4.04	2.19
.00781	1.04	1.38	4.58	3.88	2.58
.01041	1.51	1.95	4.60	4.61	2.81
.01041	1.25	2.23	4.44	5.37	4.37
.01041	1.42	2.11	4.54	5.34	3.54
.01302	1.37	2.98	4.30	5.35	5.47
.01302	1.33	3.47	4.07	6.76	8.20
.01302	1.50	2.97	4.38	6.12	5.34
.01562	1.67	3.67	4.18	6.71	7.19
.01562	1.33	4.45	3.78	5.34	9.84
.01562	1.67	4.17	4.18	6.90	7.34
.01822	1.46	5.42	3.53	5.15	11.48
.02083	1.54	6.42	3.46	4.24	12.50
.02083	1.58	6.50	3.56	4.63	11.50
.04167	1.42	16.30	2.84	2.56	26.30
.04167	1.54	16.80	2.87	2.83	25.40
.04167	.46	20.20	2.71	1.29	50.00
.04167	.23	22.30	2.66	1.04	75.80
.04167	.25	21.30	2.67	1.03	70.00
.12500	.79	67.10	2.68	1.14	73.80
.12500	.58	70.40	2.60	1.01	87.50
.12500	.46	73.70	2.58	1.18	121.30

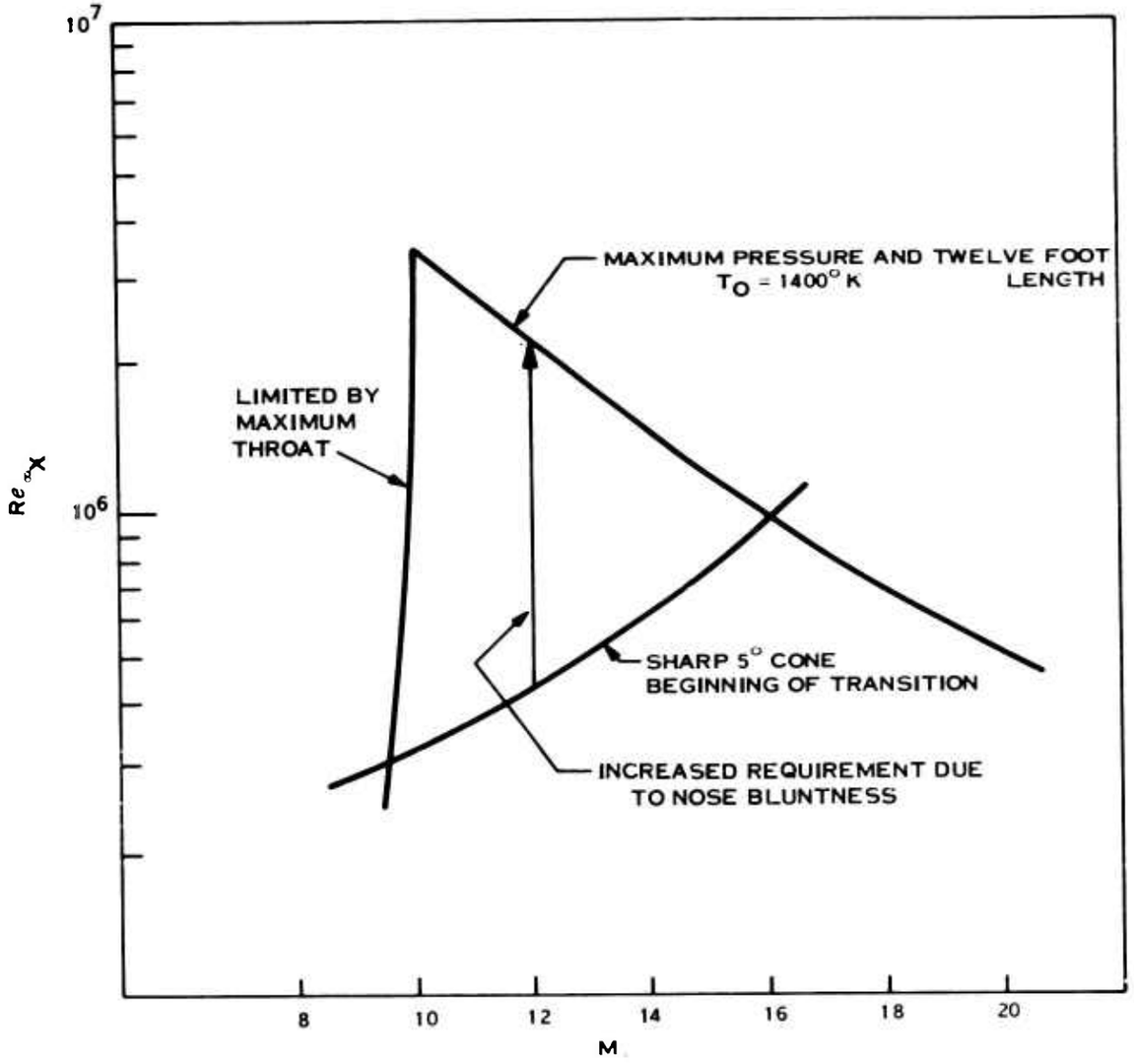

Figure 1. Tunnel capability compared to requirements for transition testing

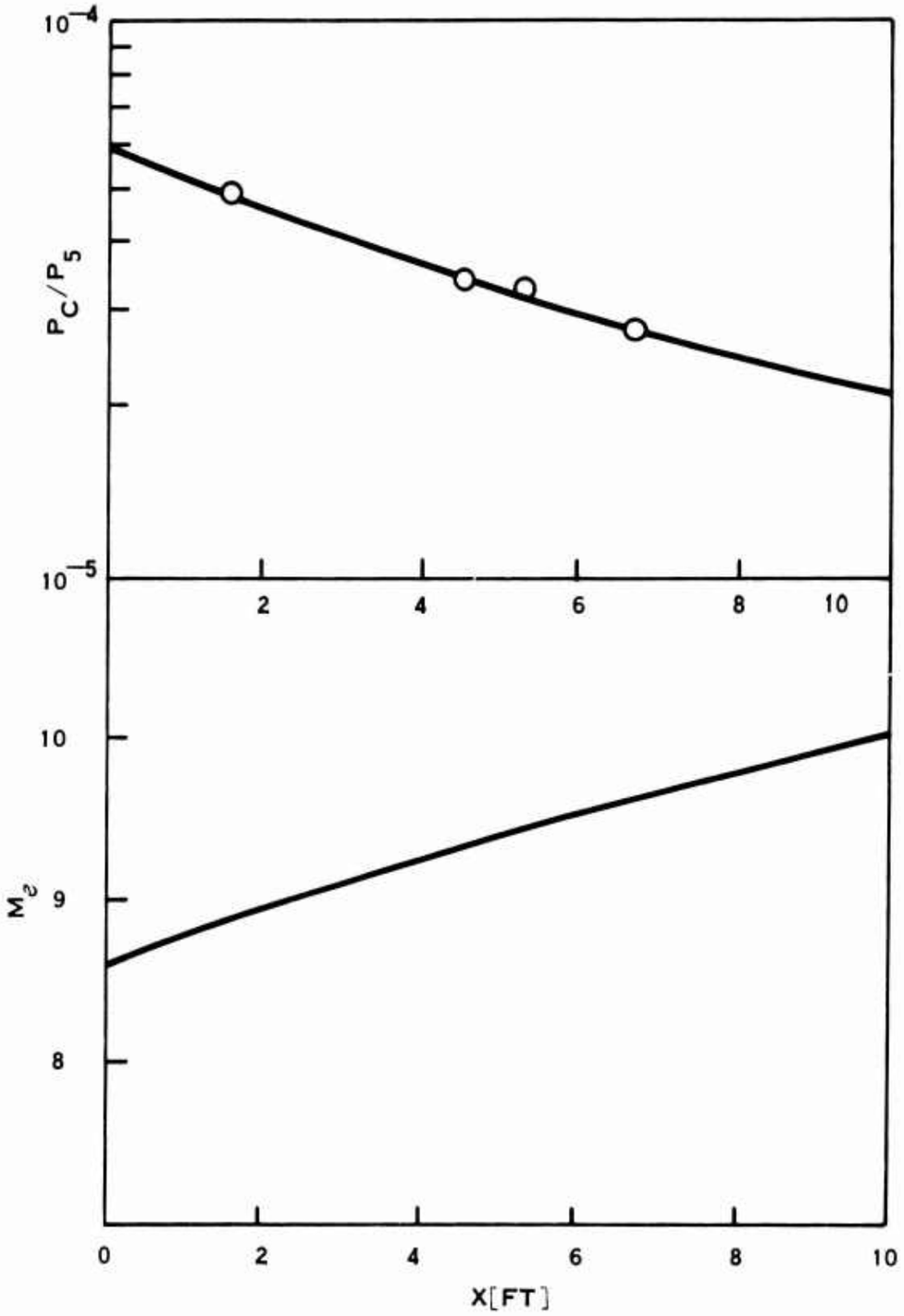

Figure 2. Typical pressure distribution along cone, $M_\infty = 10$, $R_N = 0$

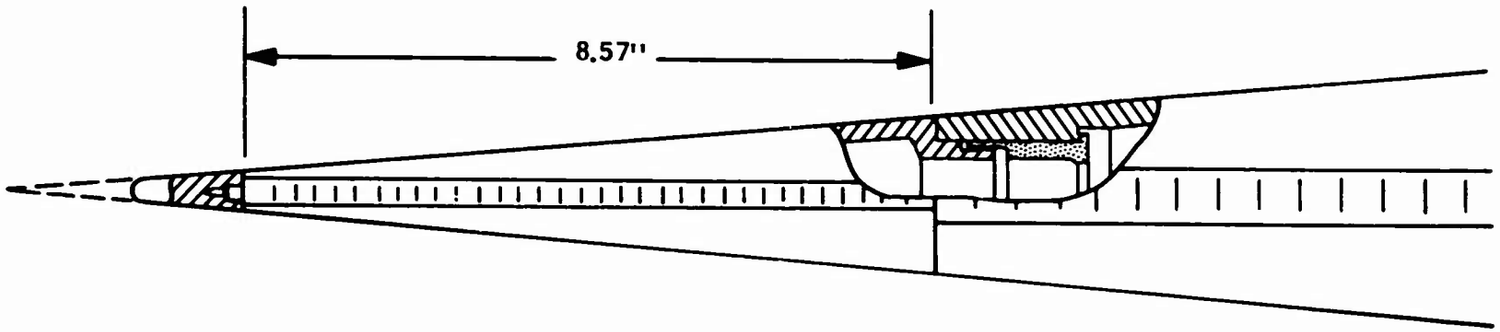

Figure 3. Sketch of modified nose section

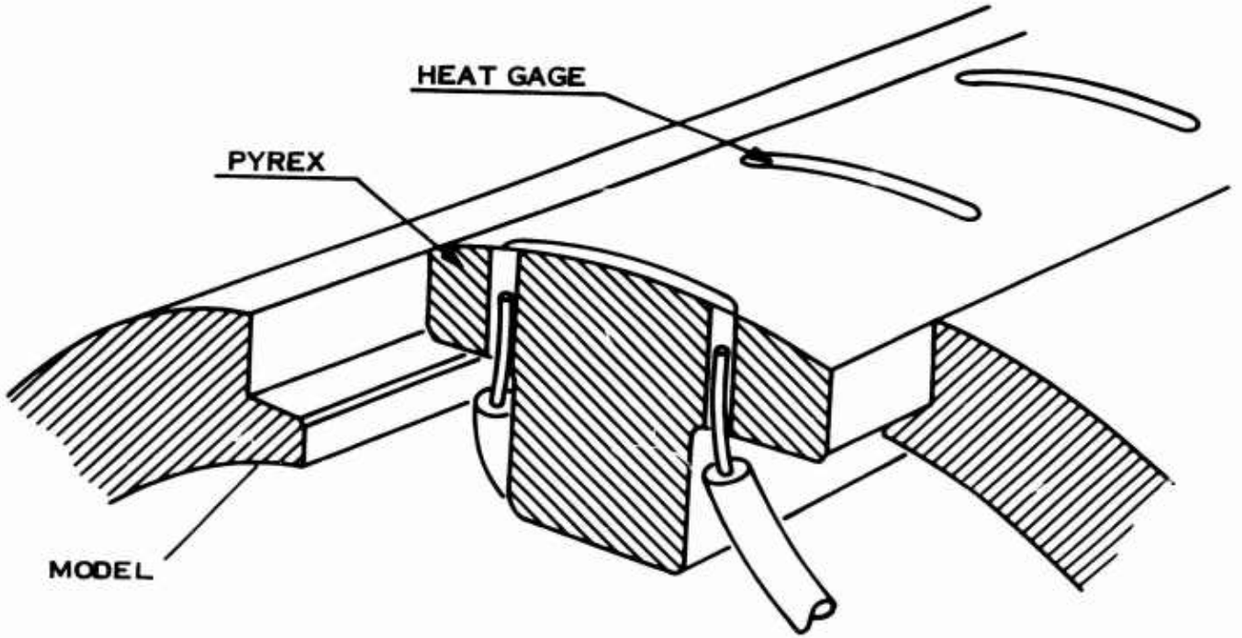

Figure 4. Construction of modified nose section

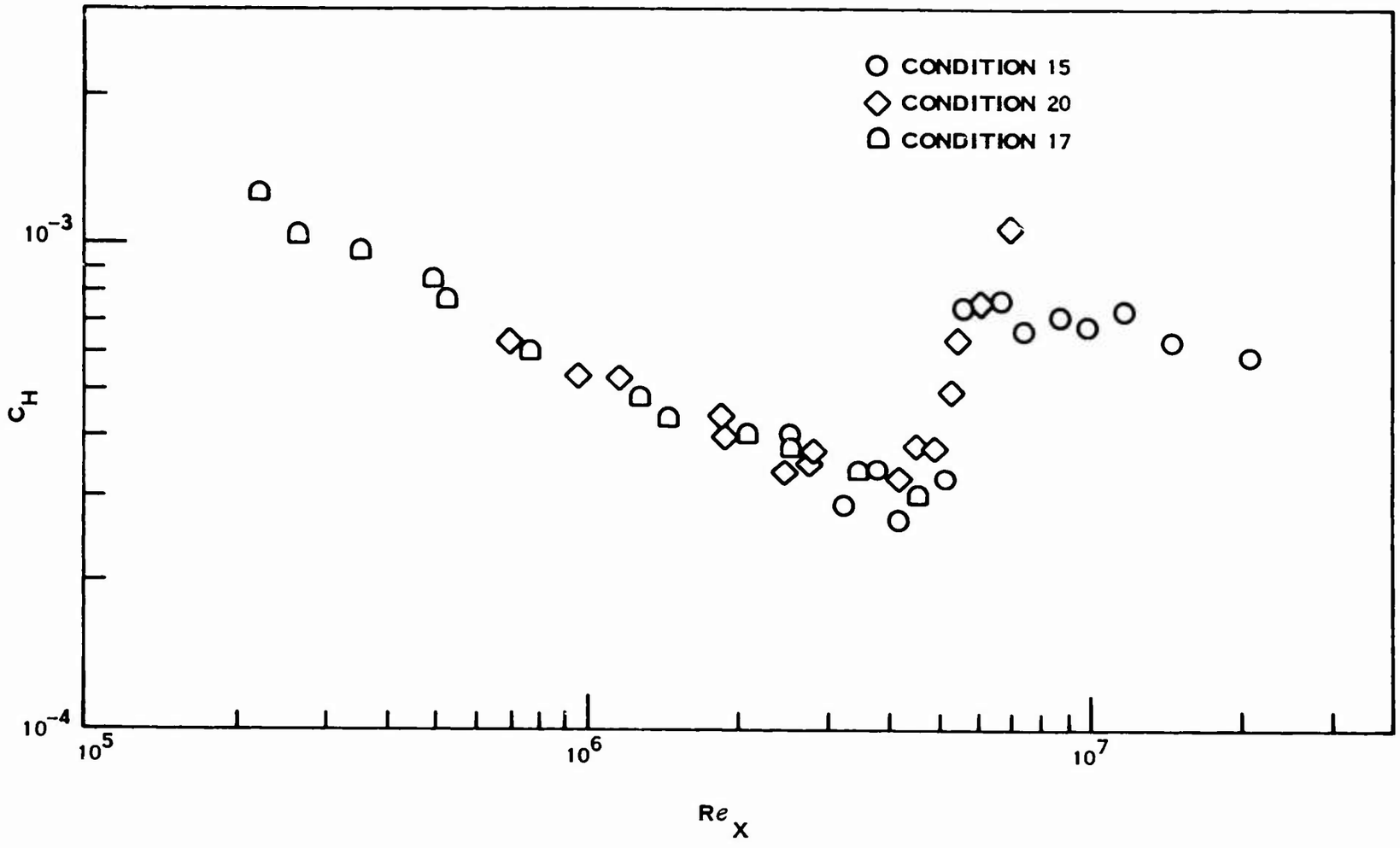

Figure 5. Non-dimensional heat transfer for three unit Reynolds numbers

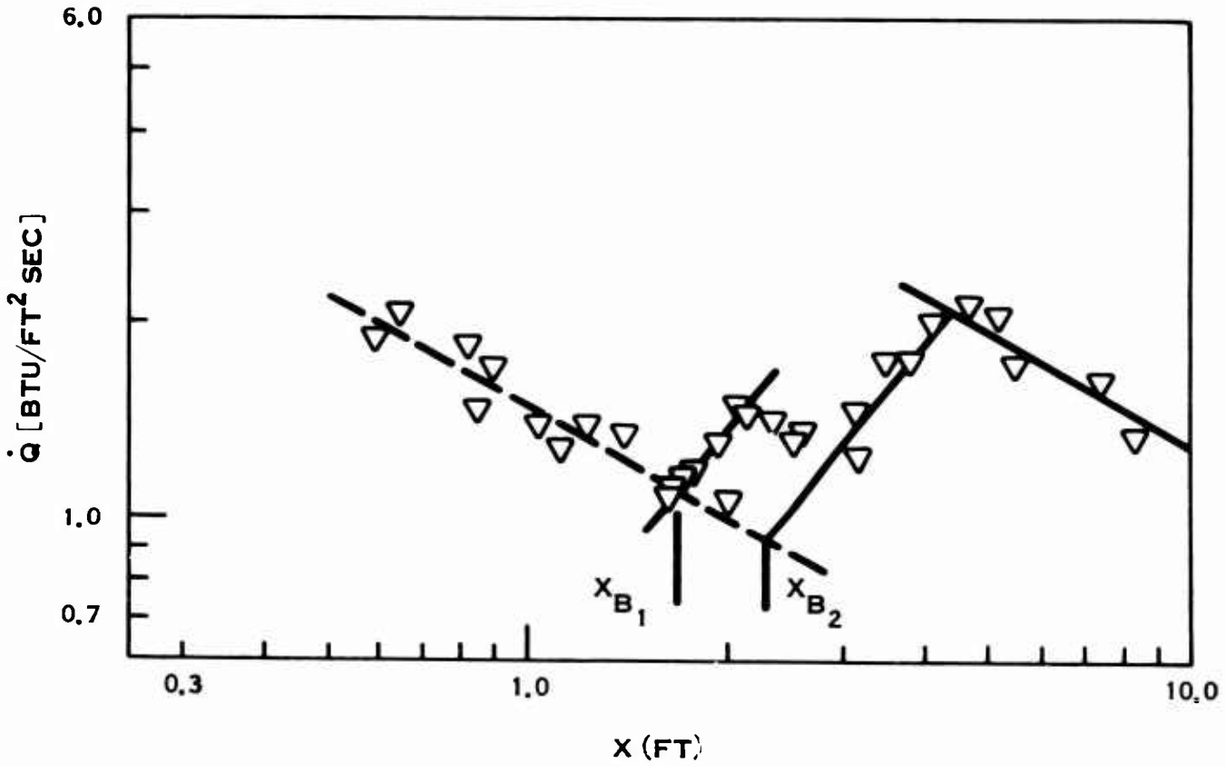

Figure 6. Heat transfer distribution (Condition 16)

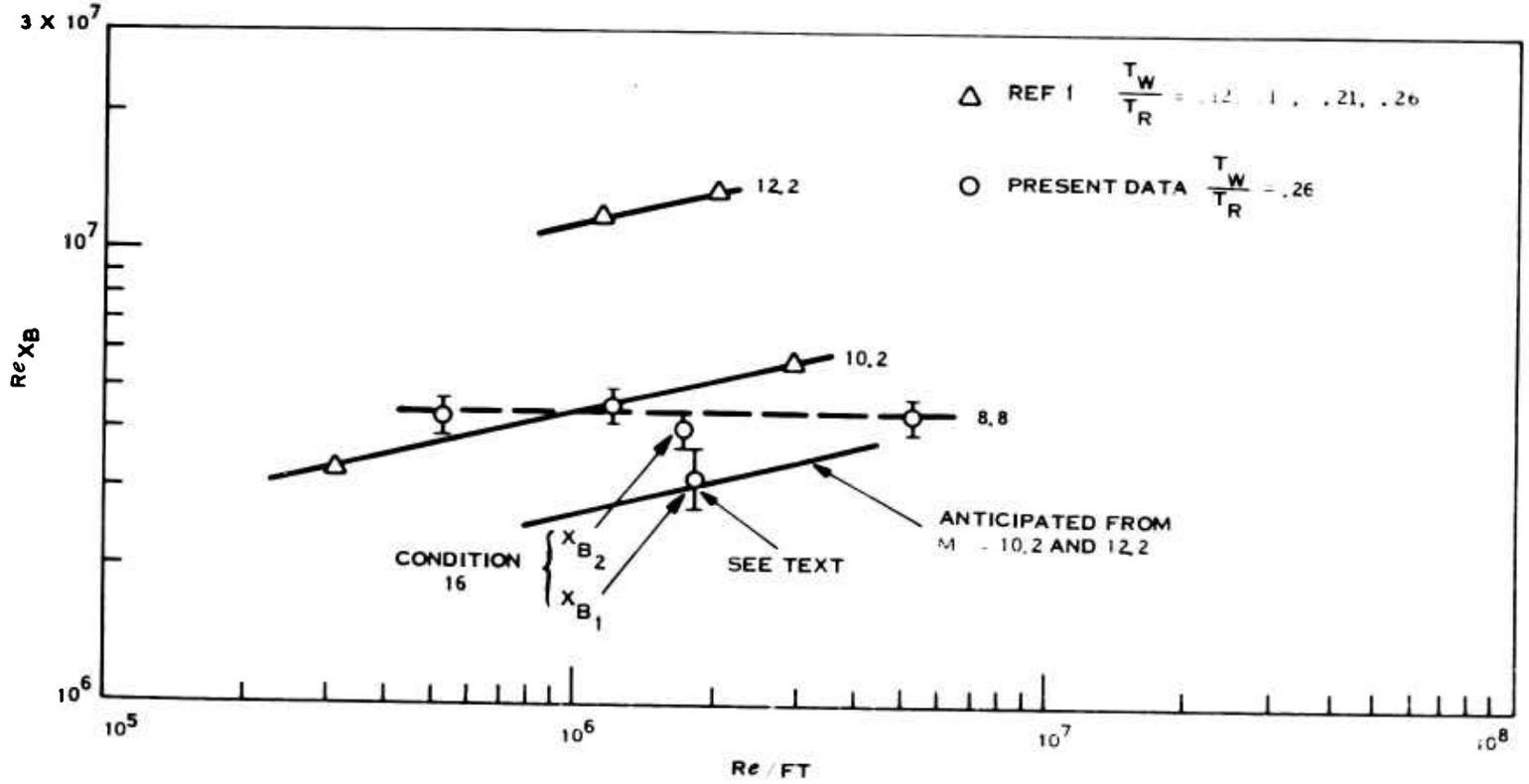

Figure 7. Transition Reynolds number as a function of unit Reynolds number

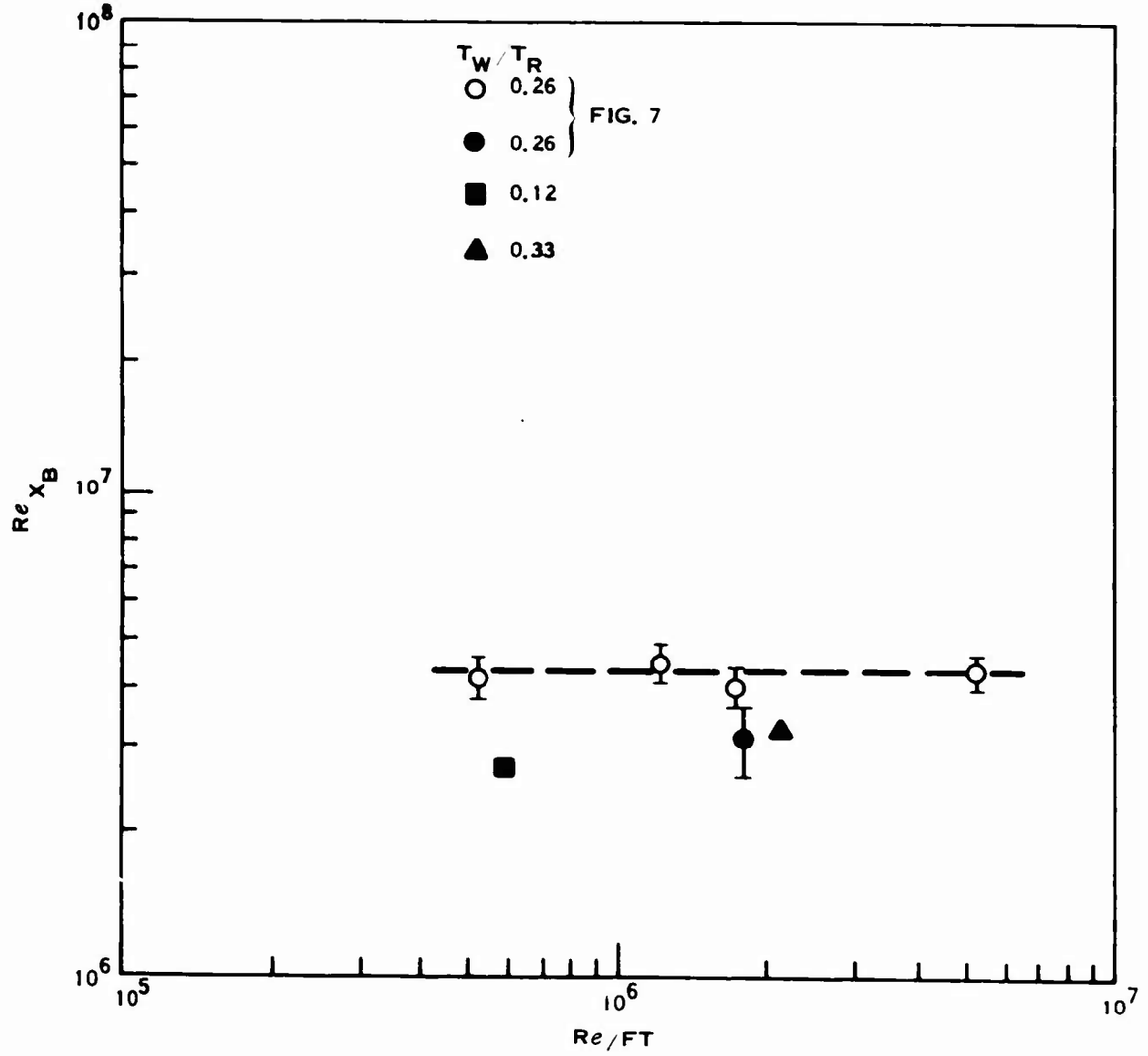

Figure 8. Transition Reynolds number at M = 10 and other wall temperature ratios

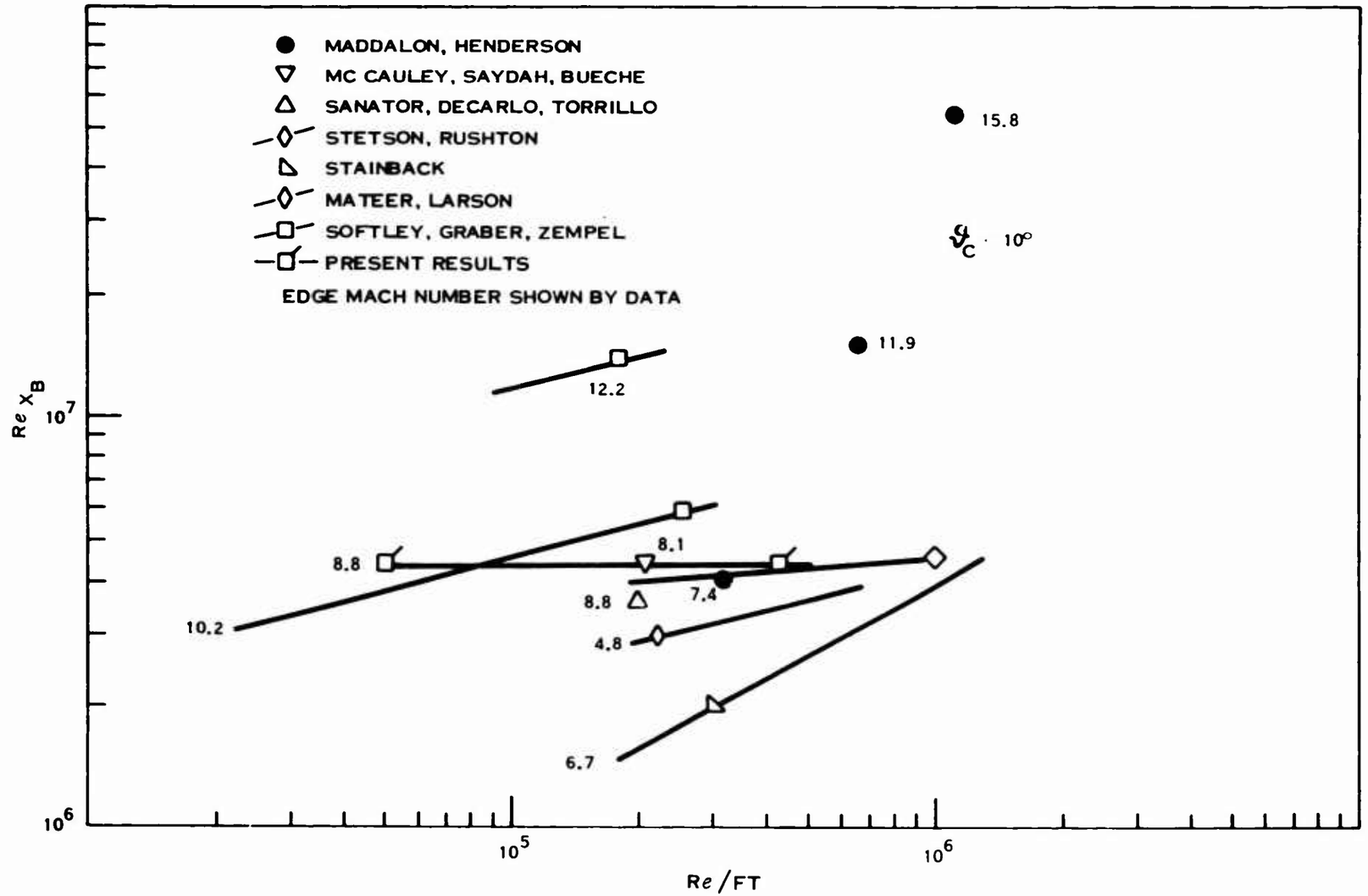

Figure 9. Continued correlation of hypersonic sharp slender cone transition

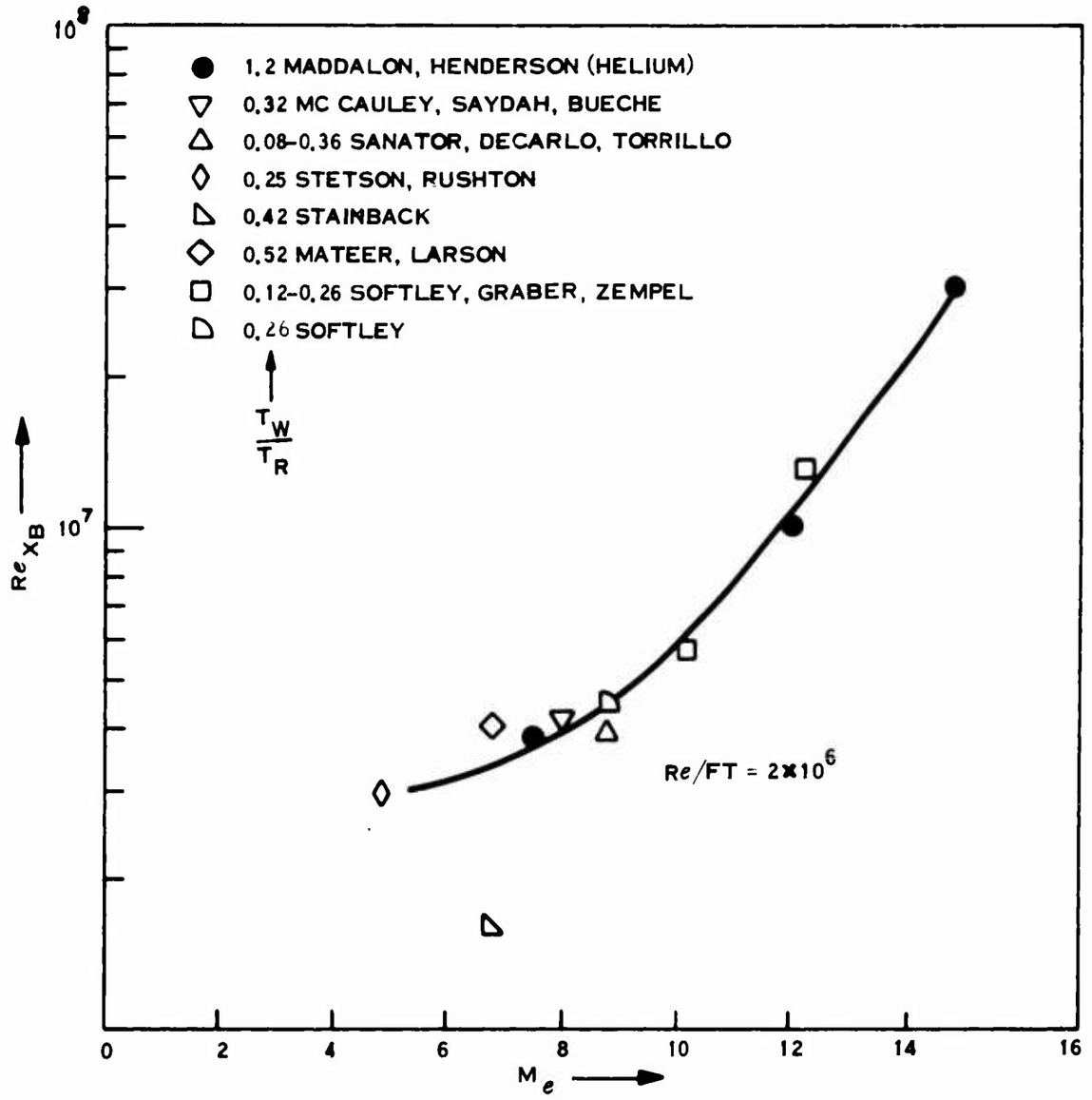

Figure 10. Transition on sharp cone as a function of local Mach number

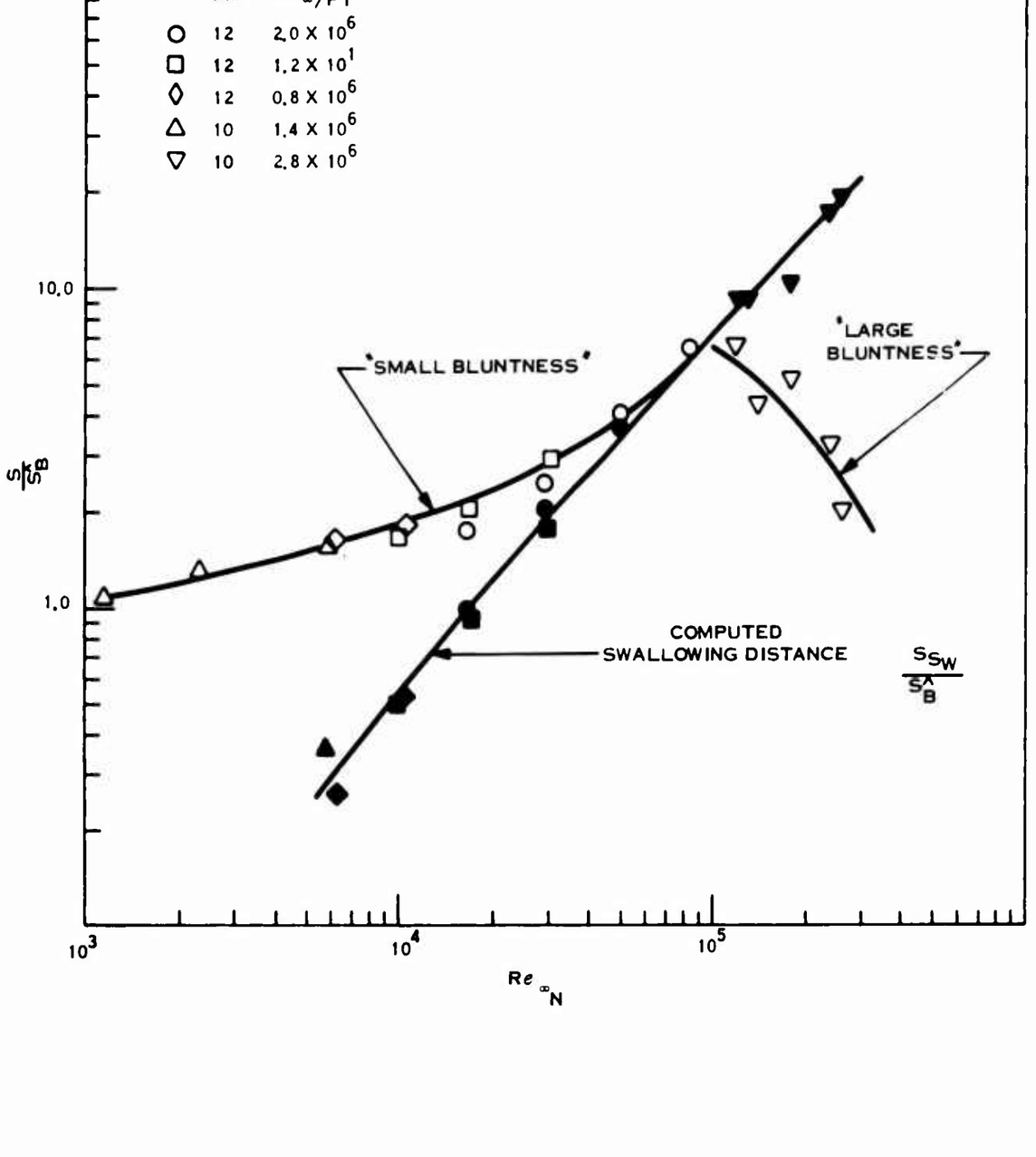

Figure 11. Transition location on blunt cones

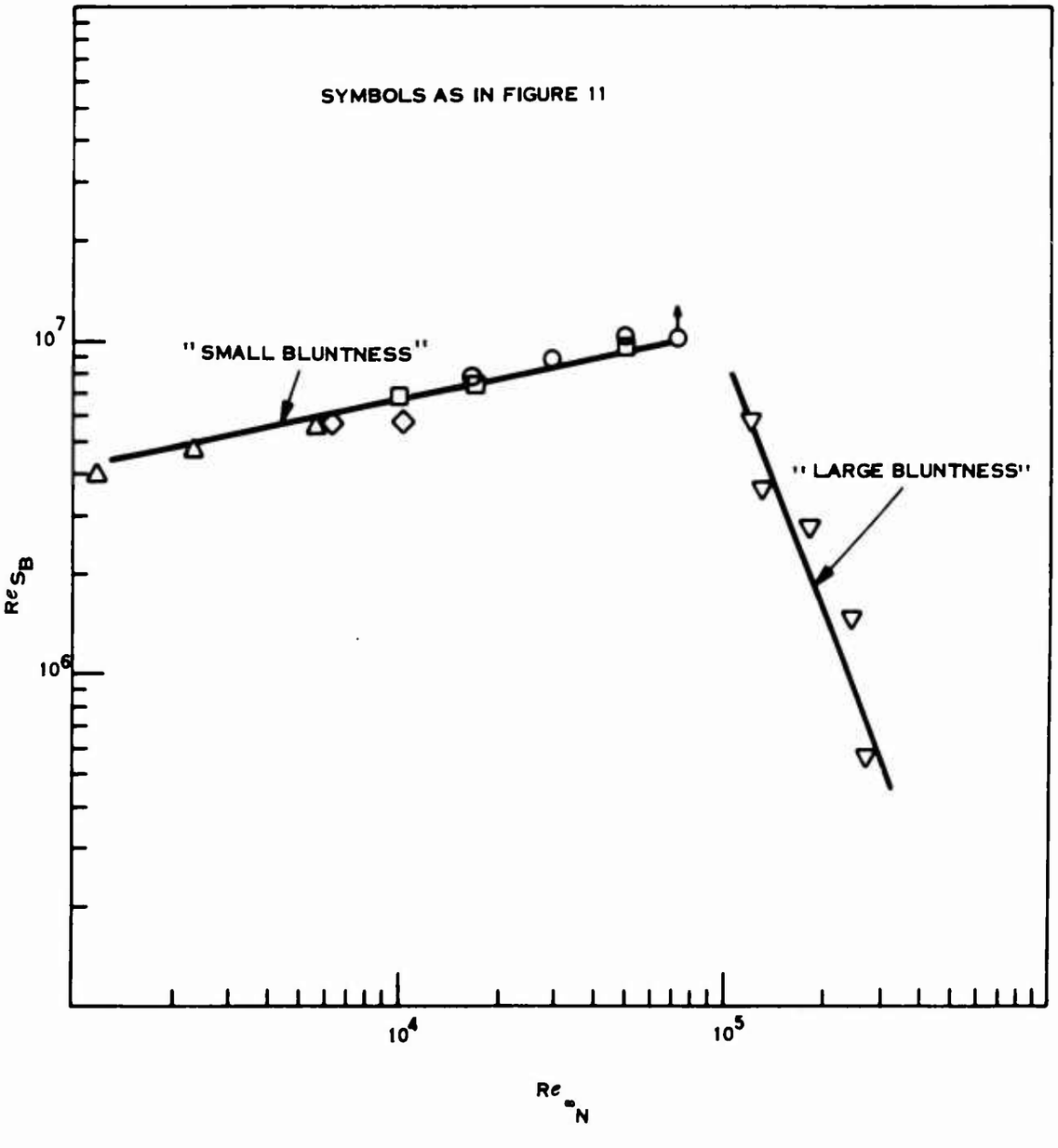

Figure 12. Transition Reynolds numbers on blunt cone

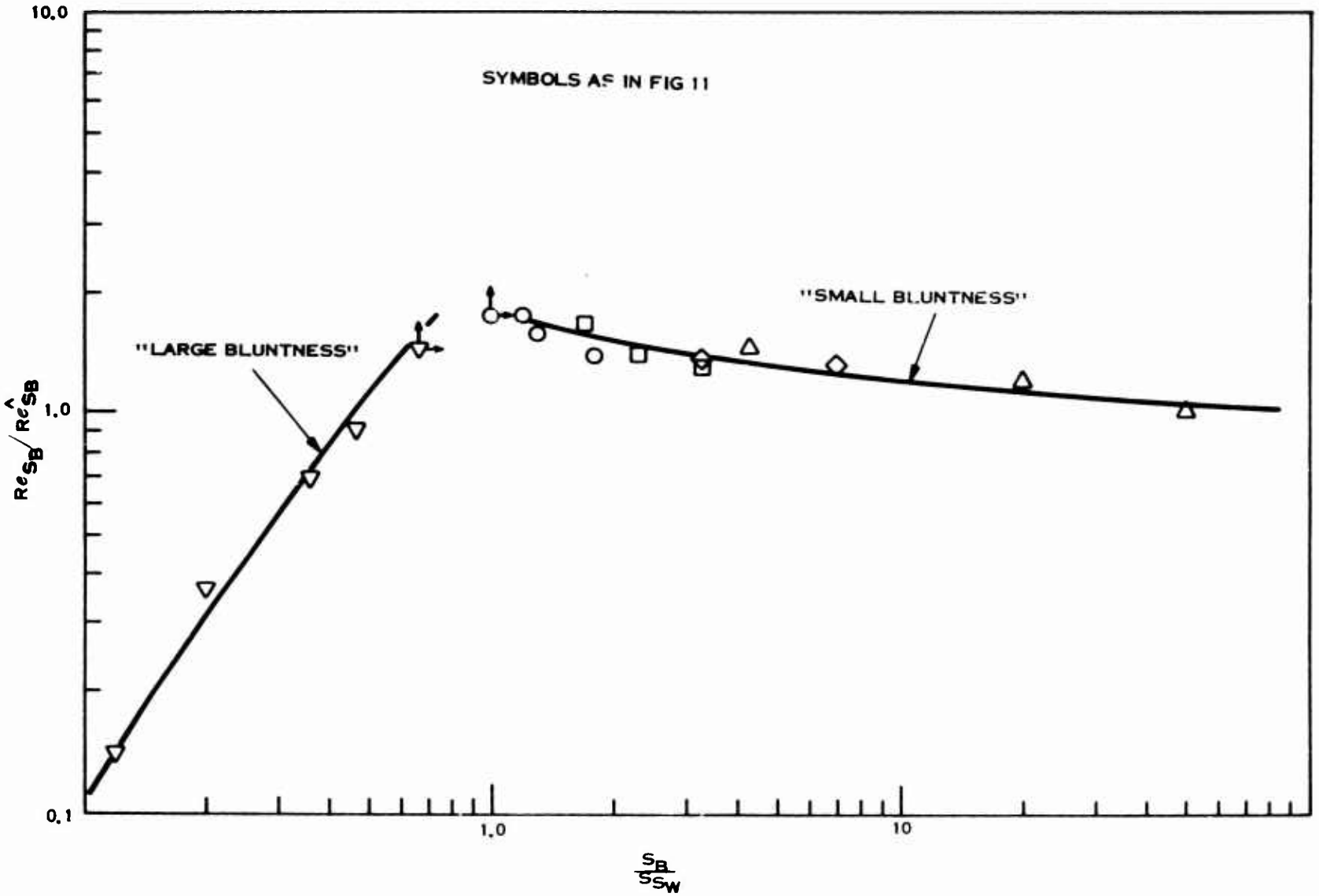

Figure 13. Blunt cone transition as a function of S_B/S_{sw}

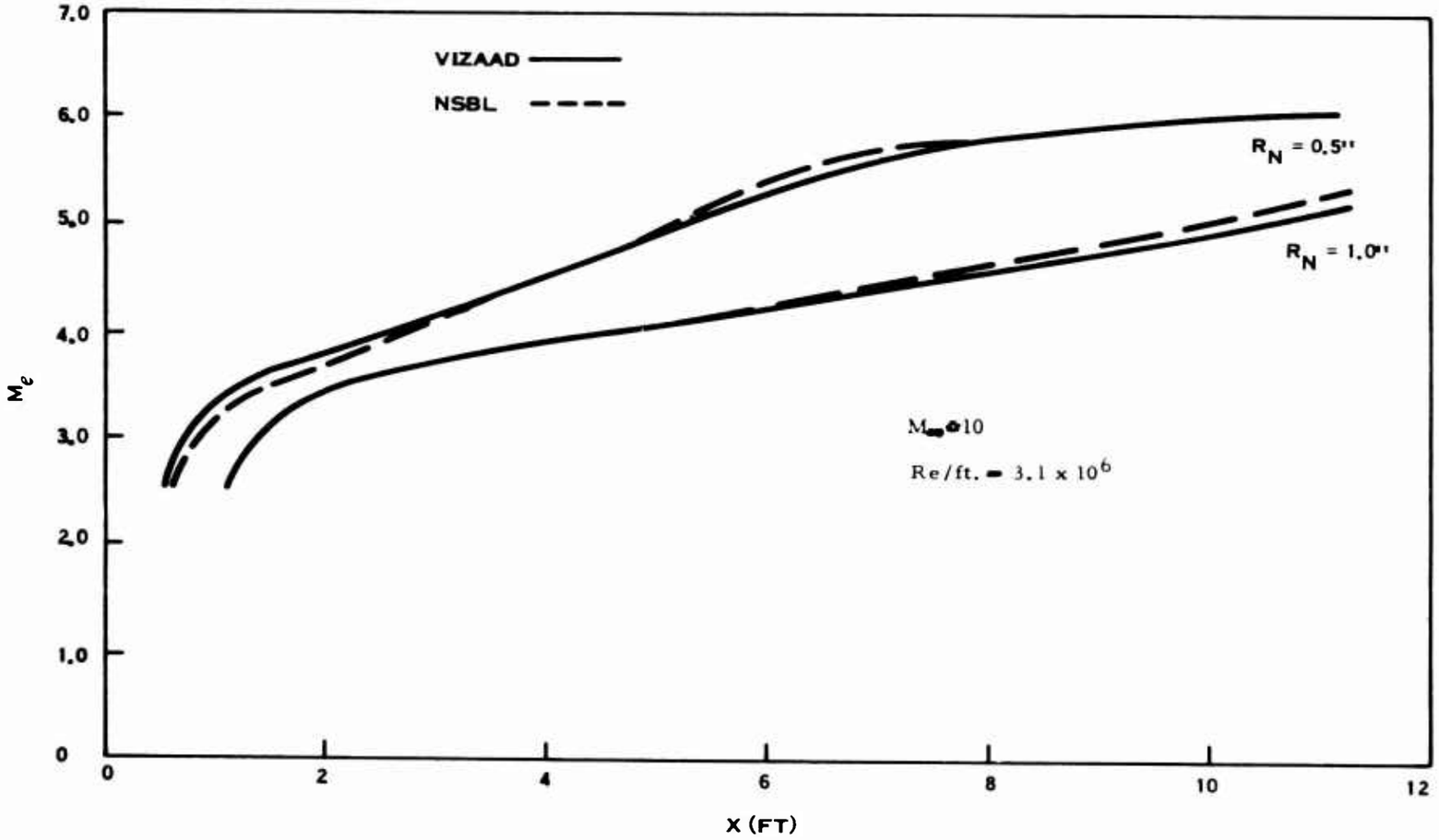

Figure 14. Comparison of edge Mach number for two calculating techniques

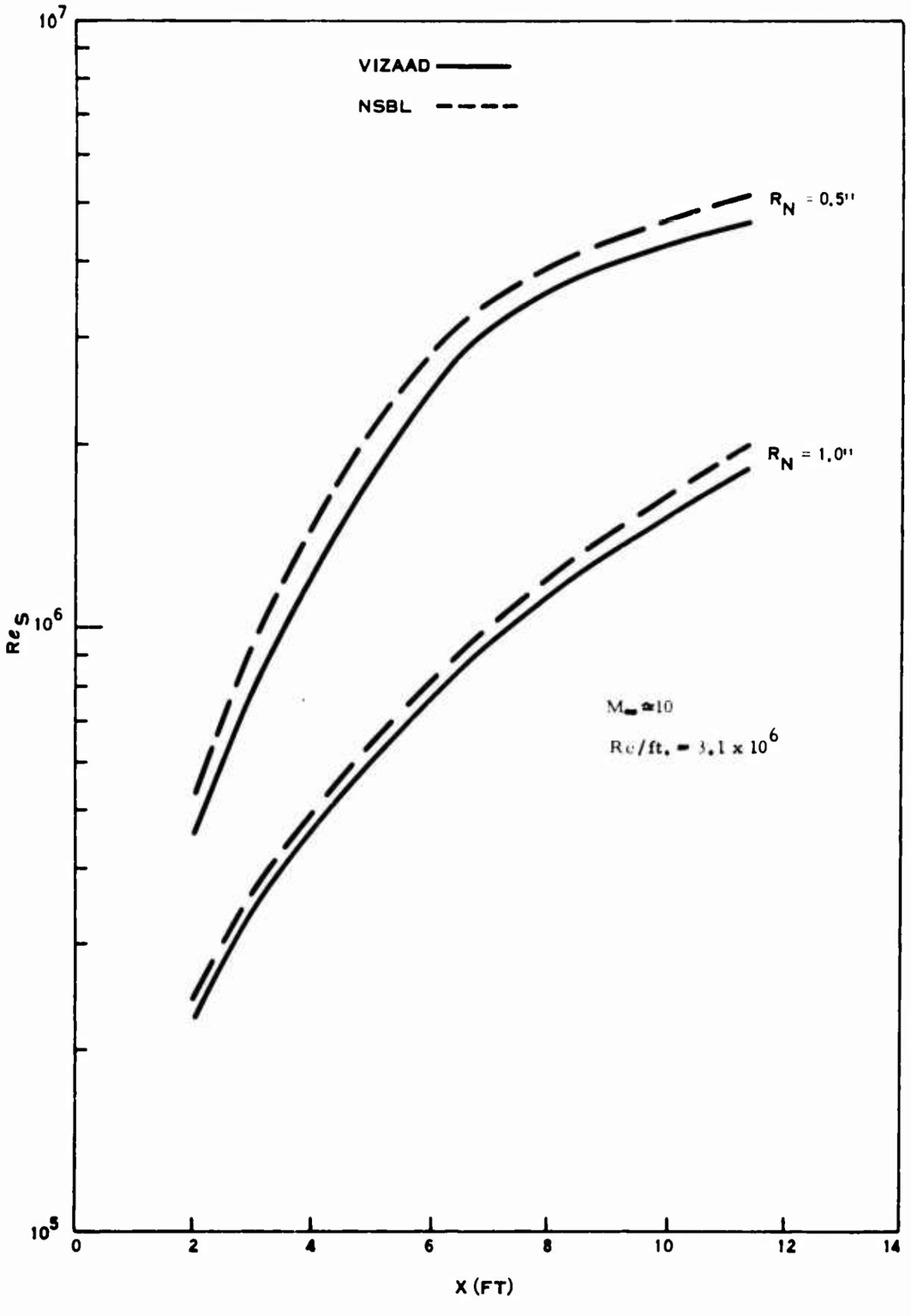

Figure 15. Comparison of edge Reynolds number for two calculating techniques

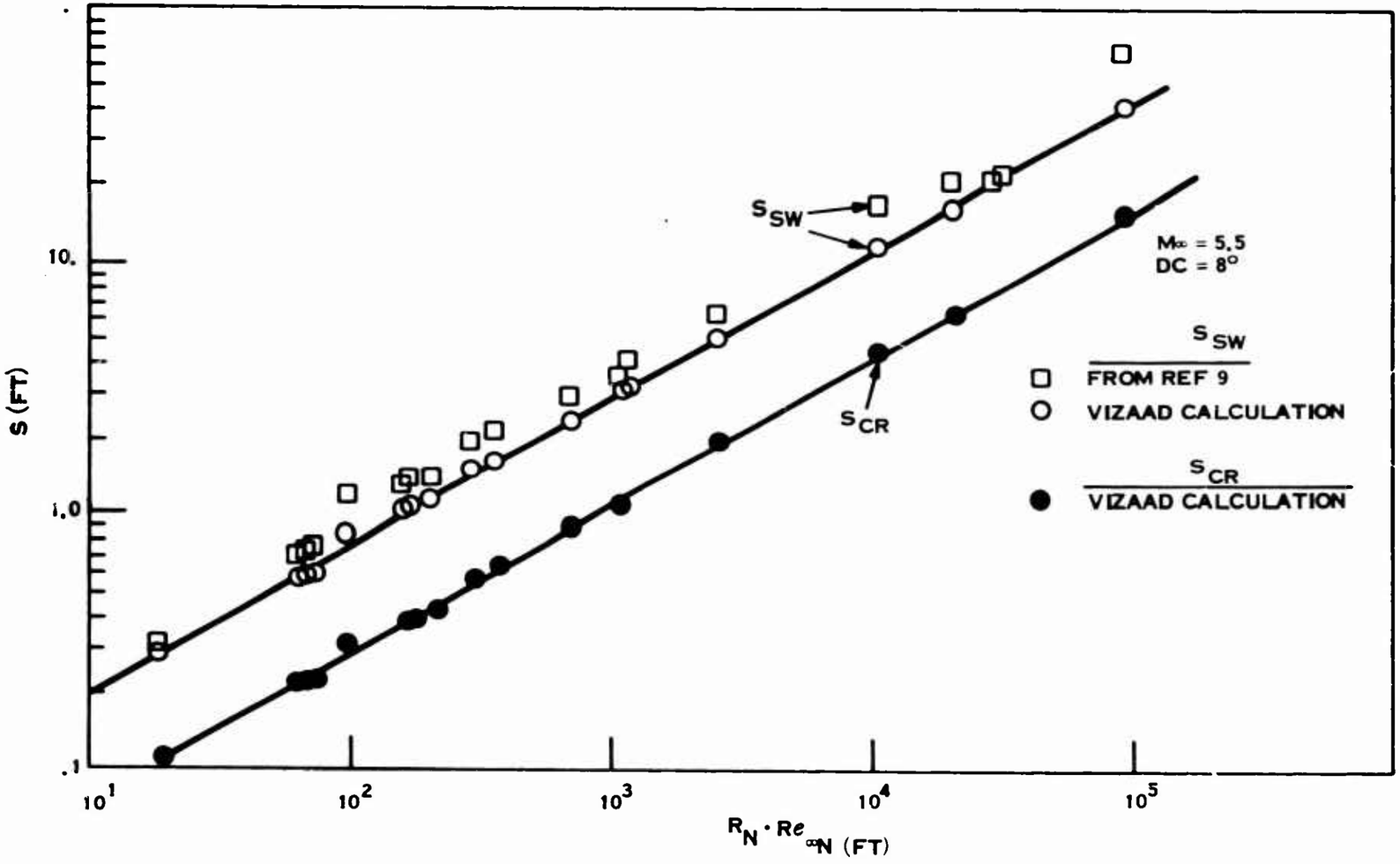

Figure 16. Swal' .ing and critical distances for $\vartheta_c = 8^\circ$, $M_\infty = 5.5$ (Ref. 9)

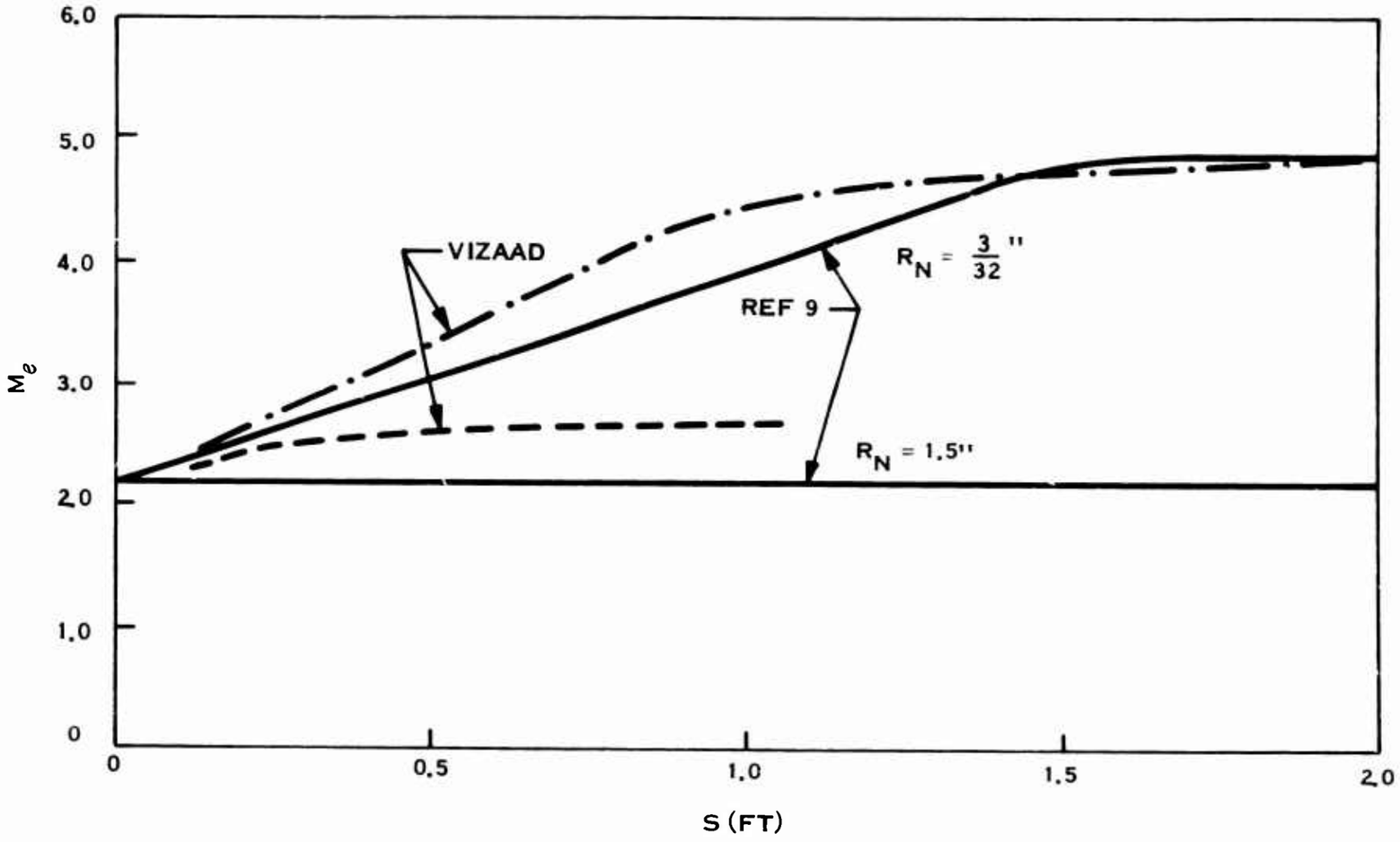

Figure 17. Comparison of M_e for $\vartheta_c = 8^o$, $M_\infty = 5.5$ (Ref. 9)

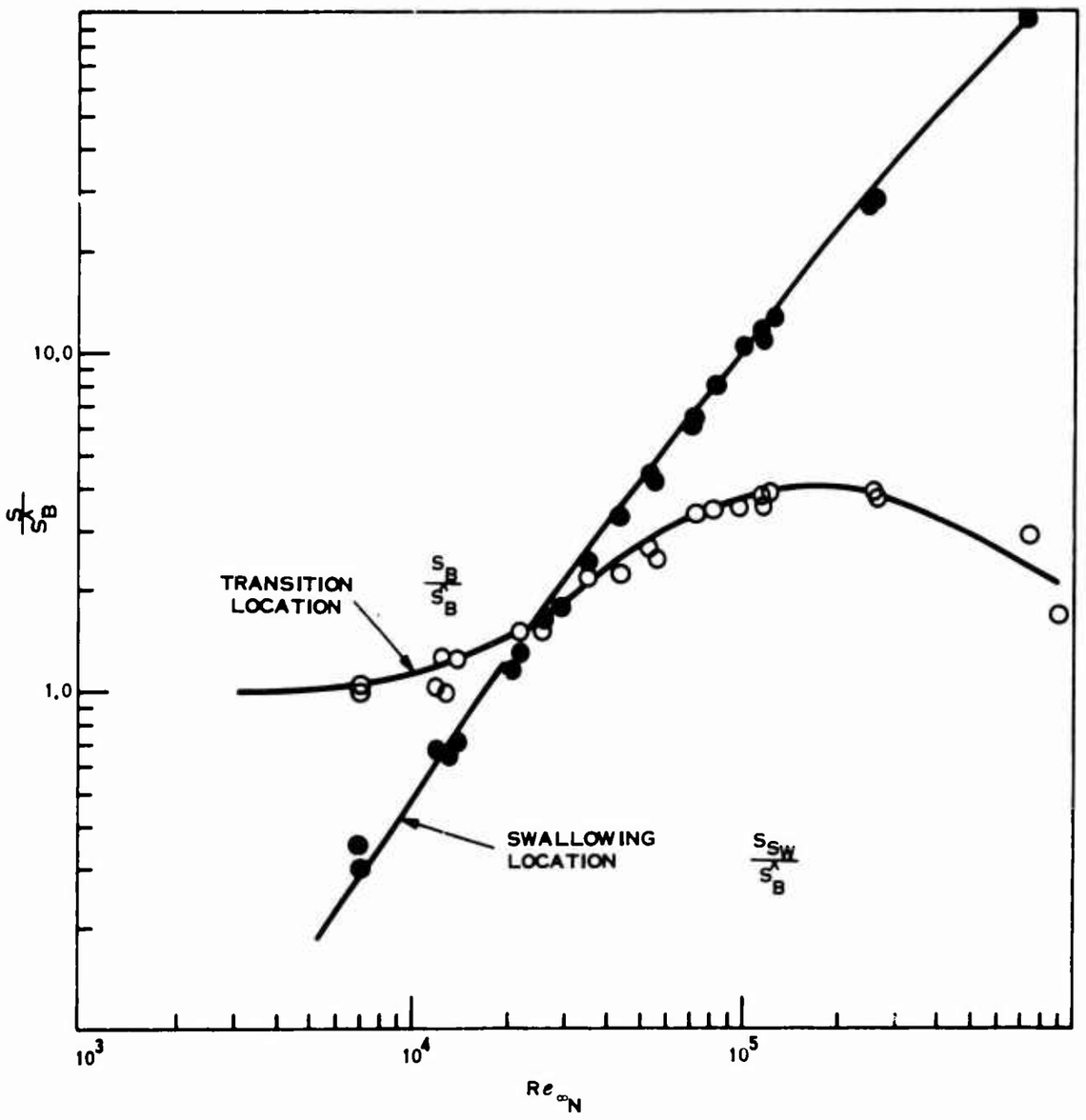

Figure 18. Transition location on blunt cone, $\vartheta_c = 8^o$, $M_\infty = 5.5$ (Ref. 9)

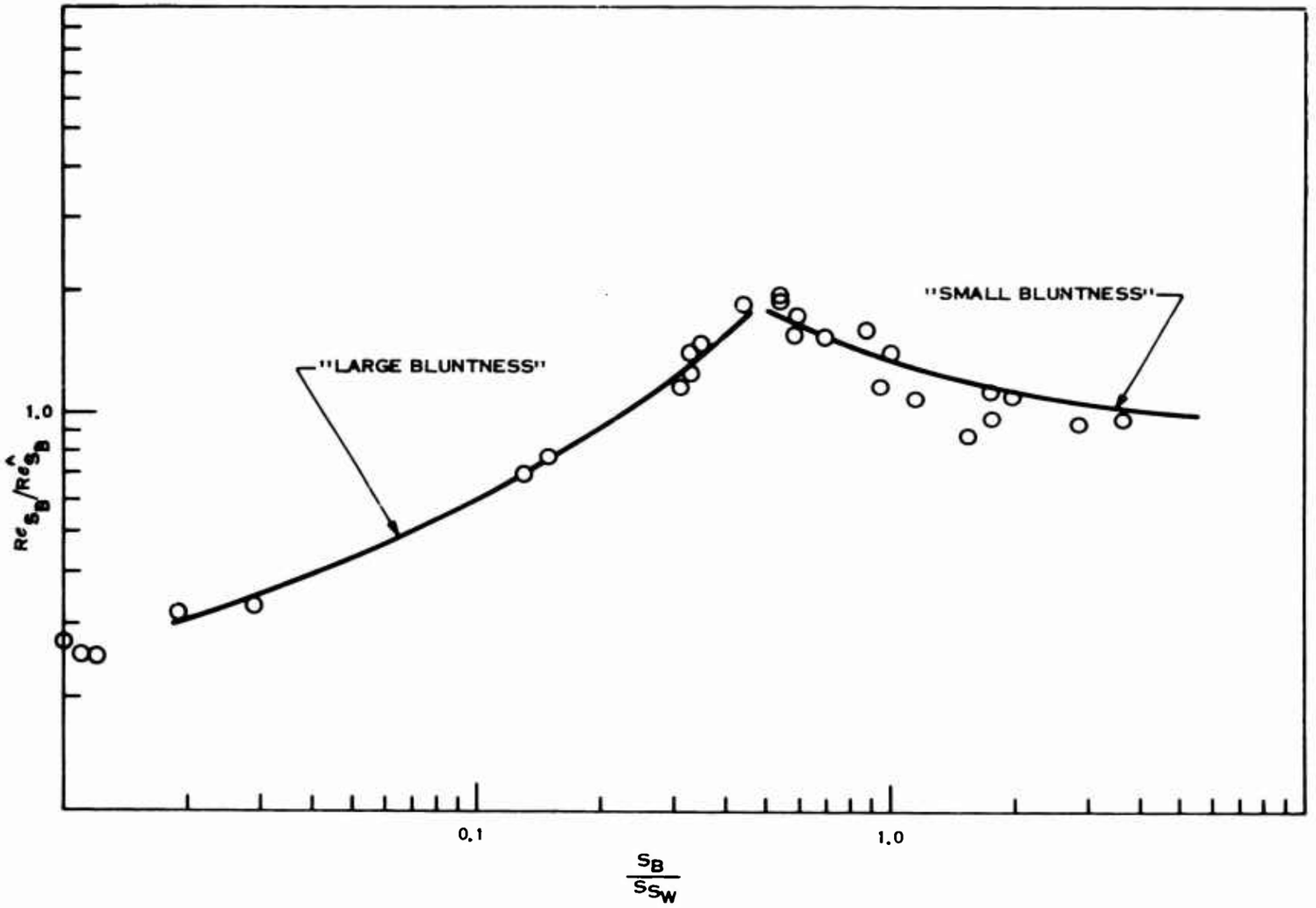

Figure 19. Transition Reynolds numbers as a function of S_B/S_{sw}, $\vartheta_c = 8^o$, $M_\infty = 5.5$ (Ref. 9)

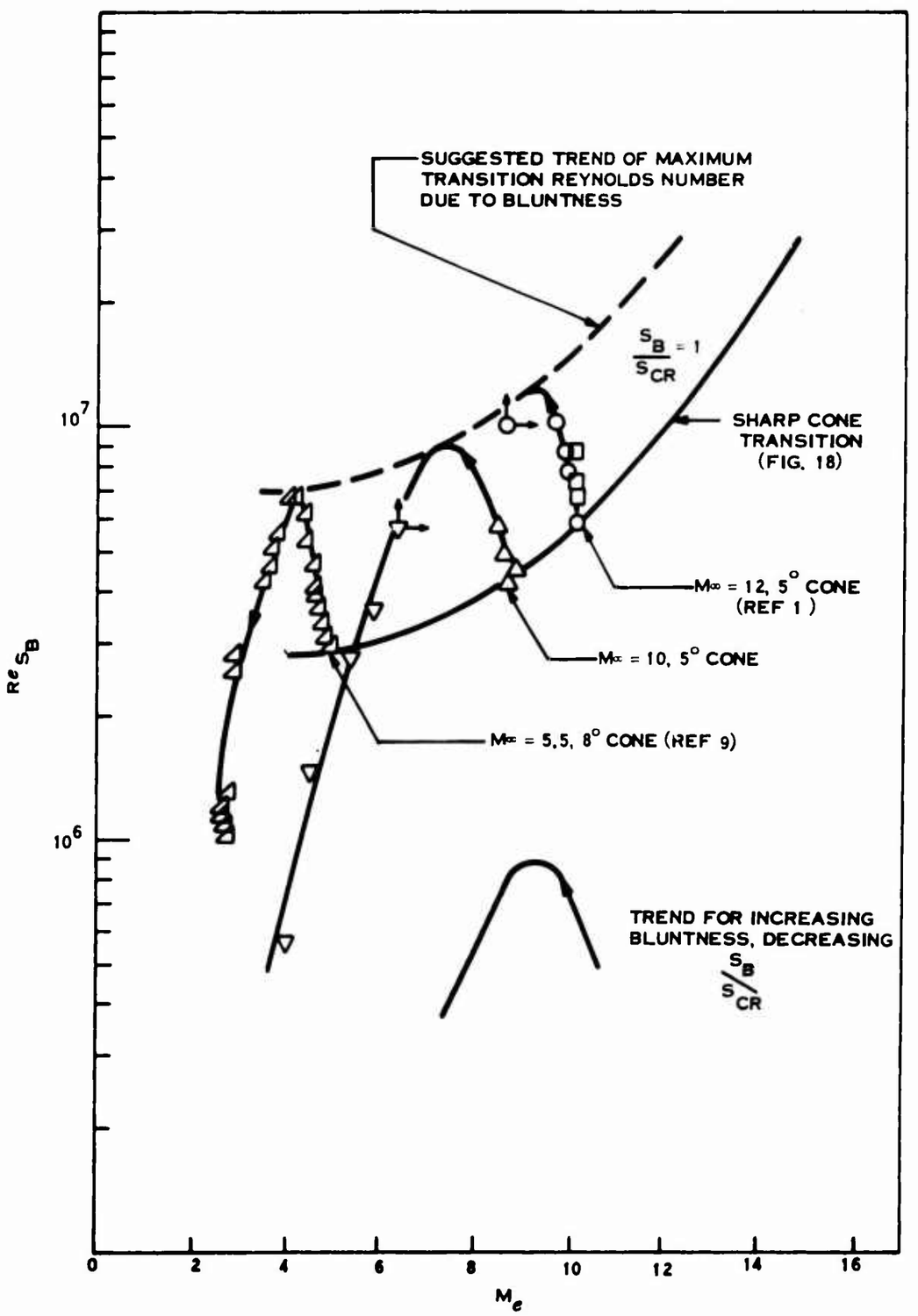

Figure 20. Transition Reynolds number on blunt cones as a function of M_e

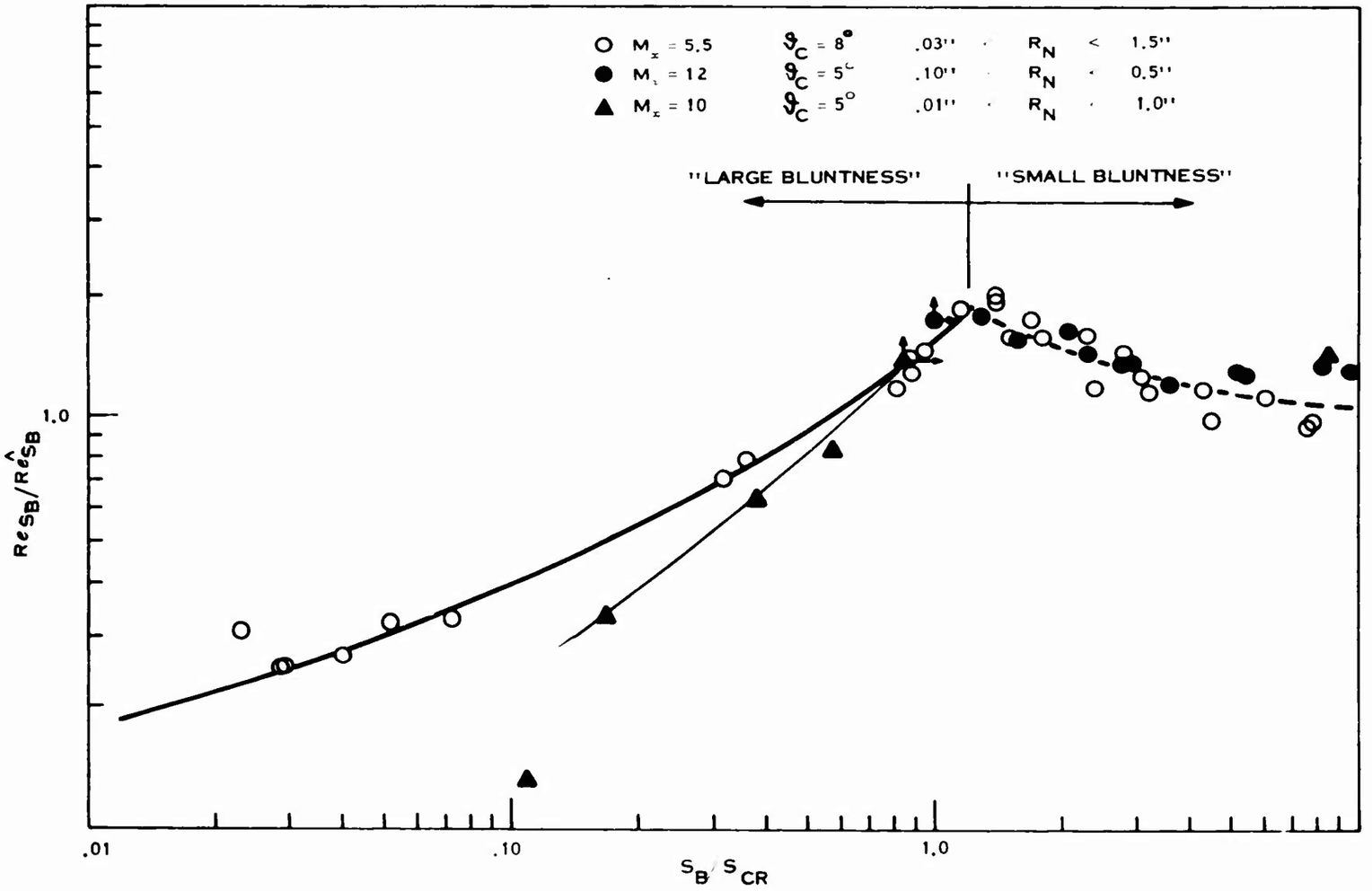

Figure 21. Blunt cone transition parameter

GENERAL ELECTRIC

SPACE SCIENCES LABORATORY
MISSILE AND SPACE DIVISION

TECHNICAL INFORMATION SERIES

AUTHOR	SUBJECT CLASSIFICATION	NO. R68SD14
E. J. Softley	Experimental Fluid Physics	DATE Oct. 1968
TITLE Transition of the Hypersonic Boundary Layer on a Cone: Part II - Experiments at M = 10 and more on Blunt Cone Transition.		G. E. CLASS I
		GOV. CLASS Unclassified
REPRODUCIBLE COPY FILED AT MSD LIBRARY, DOCUMENTS LIBRARY UNIT, VALLEY FORGE SPACE TECHNOLOGY CENTER, KING OF PRUSSIA, PA.		NO. PAGES 43

SUMMARY

Observation of transition of the hypersonic boundary layer on a cone continued with experiments at M = 10. Transition independent of the unit Reynolds number was obtained. This is dramatically different from the results obtained earlier. Blunt cone transition with a wide range of nose radii was examined. It was found possible to correlate transition on different blunt cones using a new bluntness parameter S_B/S_{or}.

KEY WORDS

Boundary layer transition
Hypersonic
Experimental

BY CUTTING OUT THIS RECTANGLE AND FOLDING ON THE CENTER LINE THE ABOVE INFORMATION CAN BE FITTED INTO A STANDARD CARD FILE

AUTHOR Eric J. Softley

COUNTERSIGNED _____